

ARTICLE

Open Access

Long non-coding RNA *MIR22HG* promotes osteogenic differentiation of bone marrow mesenchymal stem cells via PTEN/ AKT pathway

Chanyuan Jin¹, Lingfei Jia^{2,3}, Zhihui Tang¹ and Yunfei Zheng⁴

Abstract

Osteoporosis is a prevalent metabolic bone disease characterized by low bone mineral density and degenerative disorders of bone tissues. Previous studies showed the abnormal osteogenic differentiation of endogenous bone marrow mesenchymal stem cells (BMSCs) contributes to the development of osteoporosis. However, the underlying mechanisms by which BMSCs undergo osteogenic differentiation remain largely unexplored. Recently, long non-coding RNAs have been discovered to play important roles in regulating BMSC osteogenesis. In this study, we first showed *MIR22HG*, which has been demonstrated to be involved in the progression of several cancer types, played an important role in regulating BMSC osteogenesis. We found the expression of *MIR22HG* was significantly decreased in mouse BMSCs from the osteoporotic mice and it was upregulated during the osteogenic differentiation of human BMSCs. Overexpression of *MIR22HG* in human BMSCs enhanced osteogenic differentiation, whereas *MIR22HG* knockdown inhibited osteogenic differentiation both in vitro and in vivo. Mechanistically, *MIR22HG* promoted osteogenic differentiation by downregulating phosphatase and tensin homolog (PTEN) and therefore activating AKT signaling. Moreover, we found *MIR22HG* overexpression promoted osteoclastogenesis of RAW264.7 cells, which indicated that *MIR22HG* played a significant role in bone metabolism and could be a therapeutic target for osteoporosis and other bone-related diseases.

Introduction

Osteoporosis is one of the most common metabolic bone diseases which results from the disrupted balance between bone formation and resorption¹. With the progressive aging of the global population, the incidence of osteoporosis is increasing dramatically which leads to an increased risk of fractures and exerts a strong impact on morbidity, and even mortality^{2,3}. However, the pathological mechanisms of osteoporosis have not been fully understood yet. BMSCs are precursors that can

differentiate into osteoblasts and adipocytes in bone and play an important role in maintaining bone homeostasis. Previous studies showed the impaired osteogenic differentiation capacity of BMSCs contributes to the progression of osteoporosis⁴. However, the molecular basis involved in the osteogenic differentiation of BMSCs remains unclear. Therefore, a deeper insight into the mechanisms of BMSC osteogenesis will provide new strategies for treating and preventing osteoporosis.

Long non-coding RNAs (lncRNAs) are a class of non-protein-coding RNA transcripts with lengths longer than 200 nucleotides. Growing amounts of evidences have shown that lncRNAs are important regulators in diverse biological processes and diseases including osteoporosis^{5–7}. A good number of lncRNAs have been demonstrated to play critical roles in the osteogenic differentiation of BMSCs^{8–10}. For example, lncRNA *MALAT1* was

Correspondence: Zhihui Tang (tang_zhihui@live.cn) or Yunfei Zheng (yunfei_zheng@bjmu.edu.cn)

¹The Second Clinical Division of Peking University School and Hospital of Stomatology, 100081 Beijing, China

²Central Laboratory, Peking University School and Hospital of Stomatology, 100081 Beijing, China

Full list of author information is available at the end of the article
Edited by A. Stephanou

© The Author(s) 2020



Open Access This article is licensed under a Creative Commons Attribution 4.0 International License, which permits use, sharing, adaptation, distribution and reproduction in any medium or format, as long as you give appropriate credit to the original author(s) and the source, provide a link to the Creative Commons license, and indicate if changes were made. The images or other third party material in this article are included in the article's Creative Commons license, unless indicated otherwise in a credit line to the material. If material is not included in the article's Creative Commons license and your intended use is not permitted by statutory regulation or exceeds the permitted use, you will need to obtain permission directly from the copyright holder. To view a copy of this license, visit <http://creativecommons.org/licenses/by/4.0/>.

downregulated in BMSCs from osteoporosis rats compared with the normal rats, and could inhibit osteogenesis through MAPK signaling¹¹.

LncRNA *MIR22HG*, which is located on chromosome 17p13.3, has been discovered to play roles in a variety of cancers. Many previous studies revealed that *MIR22HG* exhibited tumor-suppressive role in several types of cancer including lung cancer, hepatocellular carcinoma, endometrial cancer, gastric cancer and cholangiocarcinoma, and its low expression was associated with poor prognosis^{12–17}. Conversely, some studies showed that *MIR22HG* played an oncogenic function in several cancer types such as glioblastoma, and *MIR22HG* knockdown inhibits the invasion and proliferation of cancer cells¹⁸. However, no study reported the function of *MIR22HG* in the regulation of bone metabolism.

In this study, we established osteoporosis mice model and found *MIR22HG* was significantly downregulated in mouse BMSCs (mBMSCs) from osteoporosis mice compared with the normal mice. *MIR22HG* was increased during the osteogenic differentiation of human BMSCs (hBMSCs) and acted as a positive regulator for hBMSC osteogenesis not only in vitro, but also in vivo. Mechanistically, we demonstrated that *MIR22HG* promoted osteogenic differentiation of hBMSCs via PTEN/AKT signaling. Overall, these findings suggested that *MIR22HG* might serve as a promising therapeutic target for osteoporosis treatment and prevention.

Materials and methods

Cell cultivation

Primary hBMSCs, human adipose-derived stem cells (hASCs) and RAW264.7 cells were purchased from Sciencell company (Carlsbad, CA, USA). Cells were cultured in proliferation medium (PM) consisting of DMEM supplemented with 10% fetal bovine serum and 1% antibiotics. For osteogenic differentiation, hBMSCs and hASCs were induced in osteogenic media (OM) composed of standard PM supplemented with 100 nM dexamethasone, 0.2 mM ascorbic acid, and 10 mM β -glycerophosphate. All cell-based in vitro experiments were performed at least three times.

Transfection

The recombinant lentiviruses containing full-length *MIR22HG* and the scramble control (NC) were purchased from Cyagen Biosciences (Guangzhou, China). Recombinant lentiviruses targeting *MIR22HG* (sh*MIR22HG*-1 and sh*MIR22HG*-2) and the non-targeting scramble control (shNC) were obtained from GenePharma Co. (Shanghai, China). The plasmid pcDNA3.1(+)-PTEN and pcDNA3.1(+), small interfering RNAs targeting PTEN (si-PTEN) and the scramble control (si-NC) were obtained from Integrated Biotech

Solutions Co. (Shanghai, China). The sequences are listed in Supplemental Table 1.

Alkaline phosphatase (ALP) staining and activity

ALP staining and ALP activity assay were performed as described previously¹⁹. 7 days after osteogenic induction, cells were rinsed with PBS, fixed with 4% paraformaldehyde, incubated with the NBT/BCIP staining kit (CoWin Biotech, Beijing, China). ALP activity was assayed with the ALP Activity Kit (Biovision, Milpitas, CA) and normalized to the total protein contents.

Alizarin red S staining and quantification

14 days after osteogenic induction, cells were washed with PBS, fixed with 4% paraformaldehyde, and stained with 1% Alizarin red S solution for 20 min. To quantify the degree of mineralization of hBMSCs, the stain was solubilized by cetylpyridinium chloride and quantified by a spectrophotometer at 570 nm.

RNA isolation and quantitative reverse transcription-polymerase chain reaction (qRT-PCR) analysis

Total RNA was extracted from cells with TRIzol Reagent (Invitrogen, Carlsbad, CA, USA). Then the RNA was reverse transcribed into cDNA using PrimeScript RT Reagent Kit (Takara, Tokyo, Japan). qRT-PCR was amplified with SYBR Green Master Mix (Roche Applied Science, Mannheim, Germany) on a 7500 Real-Time PCR Detection system (Applied Biosystems, Foster City, CA, USA). The comparative cycle threshold (CT) method was used to calculate the relative gene expression. The primers used for Bulge-loop reverse-transcription PCR for microRNA-22 (miR-22) and U6 were purchased from RiboBio (Guangzhou, China). The sequences of primers used are listed in Supplemental Table 1.

Western blot analysis

Cells were lysed using radioimmunoprecipitation assay (RIPA) lysis buffer. Samples were separated by electrophoresis and then transferred to PVDF membranes (Millipore, Billerica, MA, USA). The membranes were blocked with skimmed milk and incubated with primary antibodies against AKT (Cell Signaling Technology, Beverly, MA, USA), phosphorylated-AKT (Ser473) (Cell Signaling Technology), PTEN (Cell Signaling Technology) and GAPDH (HuaxingBio Science, Beijing, China) at 4 °C overnight. Then, the membranes were incubated with secondary antibodies for 1 h at room temperature. Signals were visualized using the ECL Kit (CoWin Biotech).

Establishment of ovariectomized mouse model

All animal experiments procedures were performed in compliance with the technical guidelines and approved by the Peking University Animal Care and Use Committee.

Twenty BALB/c female mice (8 weeks, 18–20 g) were purchased from Vital Co. (Beijing, China) and randomly divided to two groups: the ovariectomized (OVX) group, non-OVX control (SHAM) group. The mice in the OVX group received bilateral ovariectomy surgery. As a control, the mice in the SHAM group were subjected to removal of adipose tissue near the ovaries. After 6 weeks, mice were sacrificed under anesthesia and the femurs or tibias were collected for the related assays.

mBMSCs were isolated and purified from the tibias of SHAM and OVX mice as described previously²⁰. Flow cytometry analysis sorting was performed to screen mBMSCs which were positive for CD44 and CD29 but negative for CD45. The multilineage differentiation potential of isolated mBMSCs was evaluated via osteogenic differentiation and adipogenic differentiation. For osteogenic differentiation, mBMSCs were induced in OM for 7 days and ALP staining was performed. For adipogenic differentiation, mBMSCs were cultured in standard PM supplemented with 50 nM insulin, 100 nM dexamethasone, 0.5 mM 3-isobutyl-1-methylxanthine, and 200 mM indomethacin for 14 days. Oil red O staining was performed as described before²¹.

Micro CT analyses of mice

Six weeks after the ovariectomy surgery, femurs were harvested and scanned using a Micro CT system (pixel size 8.82 μ m, working voltage 80 kV, working current 500 mA, exposure time 1500 ms). Three-dimensional reconstruction was performed with multimodal 3D visualization software (Inveon, Siemens, Munich, Germany). Bone volume/total volume (BV/TV), trabecular number (Tb.N), and trabecular spacing (Tb.Sp) in the trabecular region (1.5 mm distal to the proximal epiphysis) were analyzed using an Inveon Research Workplace (Siemens). Then the femurs were decalcified in 10% ethylene diamine tetraacetic acid (EDTA) and stained with hematoxylin and eosin (HE).

Ectopic bone formation in vivo

The hBMSCs infected with lentivirus were induced in OM for 7 days before the in vivo experiments. Next, 5×10^6 cells were mixed with 7 mm \times 5 mm \times 2 mm Bio-Oss Collagen (Geistlich, GEWO GmbH, Baden-Baden, Germany), incubated for 1 h at 37 °C, and then implanted subcutaneously into the dorsal surface of 8-week-old BALB/c homozygous nude (nu/nu) female mice ($n = 6$ per group). The mice were randomized into 5 groups: shNC-hBMSCs/Collagen group, shMIR22HG-1-hBMSCs/Collagen group, shMIR22HG-2-hBMSCs/Collagen group, NC-hBMSCs/Collagen group and MIR22HG-hBMSCs/Collagen group. The implants were collected after 8 weeks and fixed with 4% formalin, decalcified, and embedded in paraffin wax. Sections (5 μ m)

were cut and stained with HE, Masson's trichrome and immunohistochemical analysis. Immunohistochemical analysis was performed to detect the expression level of osteocalcin (OCN) (anti-OCN, Cell Signaling Technology).

RNA sequencing

Total RNA isolated from MIR22HG knockdown or shNC hBMSCs was used as input material for the RNA sample preparations. cDNA was synthesized and then PCR was performed with phusion high-fidelity DNA polymerase, universal PCR primers and index primer. Finally, PCR products were purified (AMPure XP system) and library quality was evaluated on the Agilent Bioanalyzer 2100 system. Thereafter, the clustering of the indexed samples was performed on a cBot Cluster Generation System using TruSeq PE Cluster Kit v3-cBot-HS (Illumina). After cluster generation, the library preparations were sequenced on an Illumina NovaSeq platform and 150 bp paired-end reads were generated. Differentially expressed genes were defined as those with a P value < 0.05 and a Fold change > 2 .

Fluorescent in situ hybridization (FISH)

FISH was conducted with a Fluorescent In Situ Hybridization Kit (RiboBio). Briefly, cells were washed in PBS, fixed with 4% formaldehyde, and then permeabilized in PBS containing 0.5% Triton X-100 at 4 °C for 5 min. Subsequently, cells were prehybridized at 37 °C for 30 min and then hybridized with anti-MIR22HG, anti-U6, or anti-18S oligodeoxynucleotide probe at 37 °C overnight. Then the cells were stained with DAPI for detection of nuclei and captured using a confocal microscope (Carl Zeiss, Germany).

Subcellular fractionation

Nuclear and cytoplasmic fractions of hBMSCs were separated using a Nuclei Isolation Kit (Invent-biotech, Minnesota, USA). RNA was isolated from both fractions with Trizol and then reverse transcribed into cDNA. The RNA expression was quantified by qRT-PCR as described above¹⁹. MALAT1 and GAPDH were used as fractionation indicators. The primers used are listed in Supplementary Table 1.

Colocalization of MIR22HG and PTEN

The colocalization of MIR22HG and PTEN was performed as previously described²². After hybridization with an anti-MIR22HG probe (RiboBio), hBMSCs were washed with PBS and incubated with the PTEN antibody at 4 °C overnight. The next day, the cells were incubated in the dark using a Dylight 488-conjugated secondary antibody (Abbkine, California, USA) and stained with DAPI.

Tartrate resistant acid phosphatase (TRAP) staining

For osteoclast differentiation, RAW264.7 cells were treated with murine receptor activator of nuclear factor- κ B ligand (RANKL) (50 ng/ml, Peprotech, NJ, USA) for 5 days. TRAP staining was performed using an acid phosphatase kit (Sigma-Aldrich, St. Louis, MO, USA). Images of TRAP-positive multinucleated cells (containing ≥ 3 nuclei/cell) were recorded with a microscope.

Statistical analysis

All statistical values were calculated using SPSS version 16.0 (SPSS Inc., Chicago, IL, USA). Independent sample *t*-test was used to evaluate statistical differences between two groups, and one-way analysis of variance (ANOVA) was used for data of multiple groups. Results were expressed as mean \pm standard deviation. A *p* value less than 0.05 was considered statistically significant.

Results

MIR22HG was decreased in OVX mice

Recent studies indicated that osteoporosis may be caused by abnormal osteogenic differentiation of BMSCs. To investigate the pathological mechanisms of osteoporosis, we constructed osteoporotic model by ovariectomy. HE staining, Micro CT images and analyses showed that the bone trabeculae of OVX mice was remarkably decreased compared with SHAM mice (Fig. 1a–d). At the same time, mBMSCs from both SHAM and OVX mice were isolated, sorted by flow cytometry and determined with differentiation assays (Supplementary Fig. 1A–C). Based on our previous work, expression levels of several interesting genes were chosen to be measured by qRT-PCR and we found many genes were differentially expressed after ovariectomy. Among them, *MIR22HG* appeared to be one of the most differentially expressed genes. As shown in Fig. 1f, the *MIR22HG* expression level was significantly decreased in OVX mice, meanwhile the expression level of *RUNX2*, an osteogenic marker, was also significantly decreased in mBMSCs from OVX mice (Fig. 1e). These results suggested the potential involvement of *MIR22HG* in the compromised osteogenesis of osteoporotic BMSCs.

MIR22HG was increased during osteogenesis of hBMSCs

To elucidate whether *MIR22HG* plays a role in osteogenic differentiation of BMSCs, we first attempted to profile *MIR22HG* expression pattern in hBMSCs after osteogenic induction. qRT-PCR result indicated that the expression of *MIR22HG* was significantly upregulated (Fig. 2a). As expected, the mRNA levels of osteogenesis-related genes *RUNX2*, *ALP*, and *OCN* were significantly increased (Fig. 2b–d).

MIR22HG promoted osteogenic differentiation

To evaluate the function of *MIR22HG* in the osteogenic differentiation of hBMSCs, we used lentivirus to knock-down or overexpress *MIR22HG* in hBMSCs (Supplementary Fig. 2A–C). Seven days after culturing the transfected cells in PM or OM, ALP activity was significantly increased in the *MIR22HG* overexpression group but decreased in the *MIR22HG* knockdown group (Fig. 3a, b). Consistently, the mineralized nodules, as detected by ARS staining and quantification on day 14, was increased in the *MIR22HG* overexpression group but reduced in the *MIR22HG* knockdown group (Fig. 3c, d). Moreover, the mRNA levels of *RUNX2*, *ALP*, and *OCN* were decreased in the *MIR22HG* knockdown group but upregulated in *MIR22HG* overexpression group (Fig. 3e–g).

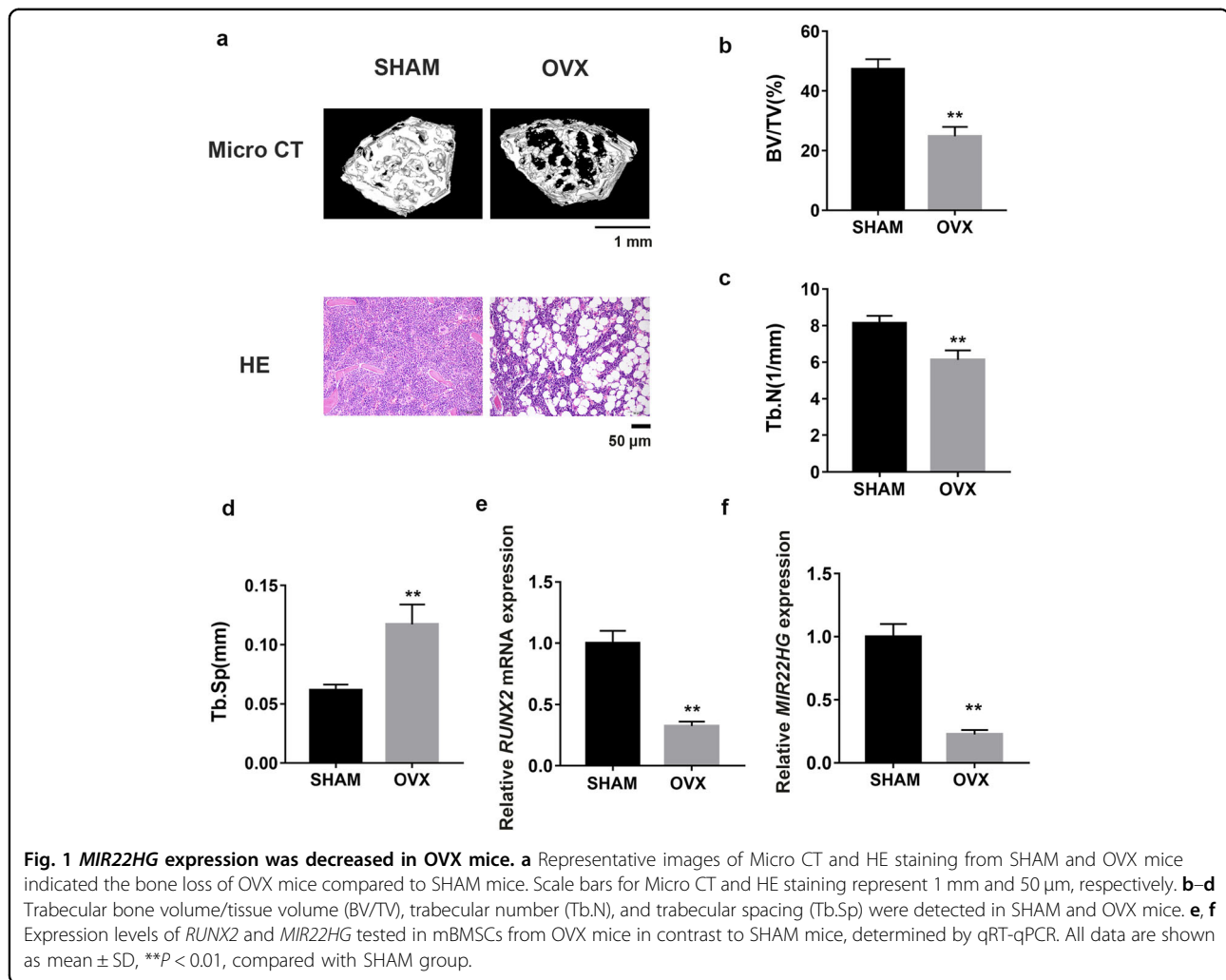
Additionally, we also investigated the effect of *MIR22HG* on osteogenesis of hASCs. Results showed *MIR22HG* played a similar function in hASCs (Supplementary Fig. 3A–F). All of these results revealed a positive role of *MIR22HG* in regulating osteogenesis.

MIR22HG promoted bone formation of hBMSCs in vivo

To further discover the role of *MIR22HG* in osteogenesis, we next tested whether *MIR22HG* could regulate bone formation potential of hBMSCs in vivo. HE staining and Masson's trichrome staining showed *MIR22HG* overexpression group formed more bone-like tissues compared with its control group (NC), whereas *MIR22HG* knockdown dramatically inhibited the efficiency of new bone formation compared with the control group (shNC). Moreover, we found the expression level of *OCN* was higher in *MIR22HG* overexpression group but lower in *MIR22HG* knockdown group as revealed by immunohistochemical staining (Fig. 4).

Differentially expressed genes in *MIR22HG* knockdown BMSCs

To further investigate the underlying mechanisms of *MIR22HG* in the regulation of hBMSC osteogenesis, sh*MIR22HG*-1, sh*MIR22HG*-2, and their negative control (shNC) hBMSCs were collected and subjected to RNA sequencing. Heat map revealed the genes that were differentially expressed following *MIR22HG* knockdown (Fig. 5a). Among these genes, 278 genes were upregulated and 112 genes were downregulated (Fig. 5b). Furthermore, KEGG pathway analysis was applied to identify the pathways that were differentially expressed by *MIR22HG* knockdown. Among the downregulated signaling pathways, phosphatidylinositol 3-kinase (PI3K)/AKT signaling which is closely associated with osteogenic differentiation appeared to be one of the most enriched pathways (Fig. 5c).



Furthermore, Western blot showed the level of p-AKT was significantly decreased in the sh*MIR22HG* hBMSCs (Fig. 6a, b), which was consistent with the result of RNA sequencing. We therefore hypothesized that *MIR22HG* might promote the osteogenic differentiation of hBMSCs with the involvement of AKT signaling.

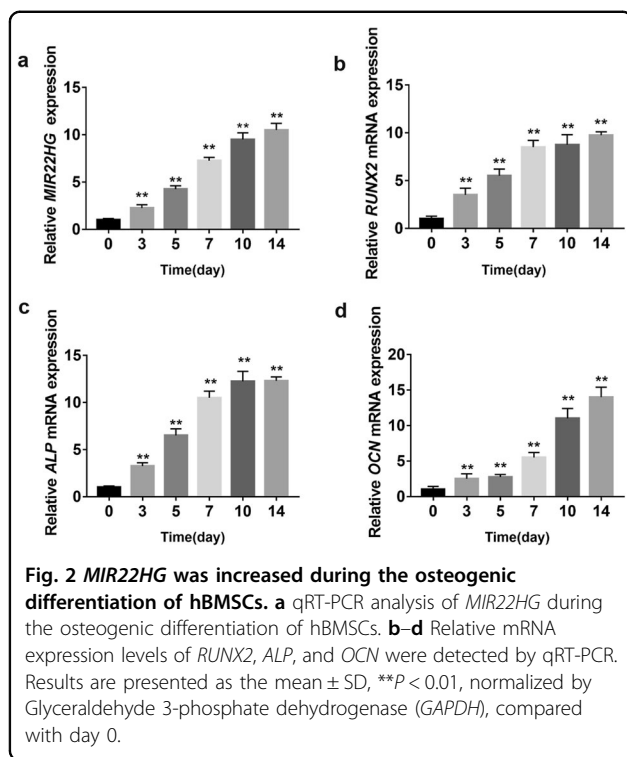
***MIR22HG* knockdown impaired osteogenesis via inhibiting AKT activation**

To determine whether *MIR22HG* knockdown inhibits hBMSC osteogenesis through inhibiting AKT signaling, we treated *MIR22HG* knockdown hBMSCs and the negative control group (shNC) with AKT signaling activator 740 Y-P. Western blot showed 740 Y-P significantly upregulated the level of p-AKT (Supplementary Fig. 4A, B). We next examined whether the addition of 740 Y-P could rescue the impaired osteogenesis caused by *MIR22HG* knockdown. ALP staining and activity showed the administration of 740 Y-P counteracted the impairments of *MIR22HG* knockdown on ALP activity (Fig. 6c,

d). Similarly, ARS staining and quantification showed 740 Y-P treatment partially abrogated the inhibitory effect of *MIR22HG* knockdown on mineralization (Fig. 6e, f). Moreover, qRT-PCR analysis revealed the addition of 740 Y-P upregulated *RUNX2*, *ALP*, and *OCN* mRNA levels in sh*MIR22HG* hBMSCs (Fig. 6g–i).

***MIR22HG* overexpression promoted osteogenesis by activating AKT signaling**

To further verify the relationship between *MIR22HG* and AKT pathway, we also investigated AKT signaling in *MIR22HG* overexpressed hBMSCs. Western blot results showed the level of p-AKT was significantly increased in *MIR22HG* overexpression group compared with NC group (Fig. 7a, b). Next, we treated *MIR22HG* overexpressed hBMSCs and its control group (NC) with PI3K/AKT inhibitor LY294002. It was found that the level of p-AKT was decreased when cells were treated with LY294002 (Supplementary Fig. 4C, D). As shown in Fig. 7c–i, inhibition of PI3K/AKT signaling pathway by



LY294002 attenuated the enhancing effect of *MIR22HG* overexpression on osteogenesis.

The role of PTEN in *MIR22HG*-mediated osteogenesis

Previous studies demonstrated that PTEN inhibits the activation of downstream proteins of AKT signaling²³, we hypothesized that PTEN played a role in the *MIR22HG*-mediated osteogenesis. Therefore, we next performed Western blot analysis of PTEN in *MIR22HG* knockdown or overexpressed hBMSCs. We found that *MIR22HG* knockdown significantly increased the level of PTEN and decreased the level of p-AKT, whereas *MIR22HG* overexpression had an opposite effect (Supplementary Fig. 5A, C). To determine the effects of PTEN in *MIR22HG*-mediated osteogenesis, we transfected sh*MIR22HG* hBMSCs and the control group (shNC) with si-PTEN. As shown in Supplementary Fig. 5B, the suppression of PTEN blocked the inhibitory effect of *MIR22HG* knockdown on ALP activity. In addition, PTEN overexpression plasmid and the empty control plasmid (PC) were introduced into *MIR22HG* overexpression hBMSCs and its control group (NC). ALP staining showed the increased ALP activity induced by *MIR22HG* overexpression was effectively reversed in the *MIR22HG* and *PTEN* double overexpressed hBMSCs (Supplementary Fig. 5D). These results suggested *MIR22HG* regulates osteogenic differentiation of hBMSCs via PTEN/AKT signaling.

The distribution of *MIR22HG*

Since the function of most lncRNAs is closely related to their subcellular location²⁴, we also investigated the distribution of *MIR22HG* of hBMSCs by FISH assay. As shown in Supplementary Fig. 6A, *MIR22HG* was mainly distributed in the nucleus of hBMSCs. Consistently, subcellular fractionation assay also demonstrated that *MIR22HG* was primarily located in the nucleus, meanwhile the marker RNAs (*MALAT1* and *GAPDH*) were enriched in their expected fractions (Supplementary Fig. 6B). Moreover, confocal microscopy for lncRNA *MIR22HG* FISH and PTEN immunostaining revealed that *MIR22HG* was localized predominantly in the nucleus, while PTEN was localized both in the cytoplasm and nucleus (Supplementary Fig. 6C). PTEN has been shown to play various roles in different cellular compartments. Nuclear PTEN is essential for maintaining chromosomal integrity and genomic stability. Cytoplasmic PTEN converts phosphatidylinositol-3,4,5-trisphosphate (PIP3) to phosphatidylinositol-4,5-bisphosphate (PIP2), thereby repressing PI3K/AKT pathway²⁵. It was reported that miR-22 reduced the level of PTEN via directly combining to the 3'UTR of PTEN²⁶. Thus, it was reasonable to hypothesize that *MIR22HG* regulated the level of PTEN through miR-22. As shown in Supplementary Fig. 6D, the level of miR-22 was significantly increased in *MIR22HG* overexpression hBMSCs. Collectively, these results indicated that *MIR22HG* might regulate PTEN through miR-22.

The role of *MIR22HG* in osteoclast differentiation

It has been demonstrated that the imbalance between osteoblastic bone formation and osteoclastic bone resorption can cause osteoporosis²⁷. Understanding the mechanisms of osteoclastogenesis is essential to develop treatments for osteoporosis. Therefore, we also investigated the role of *MIR22HG* in osteoclast differentiation. We found the expression level of *MIR22HG* was increased during RANKL-induced osteoclastogenesis of RAW264.7 cells (Supplementary Fig. 7A). Gain- and loss-of-functions studies showed *MIR22HG* promoted osteoclast differentiation of RAW264.7 cells (Supplementary Fig. 7B–E).

Discussion

Recent studies have reported that lncRNAs could act as key regulators of osteogenic differentiation and pathological processes of osteoporosis²⁸. Fei et al. reported that 51 lncRNAs were differentially expressed in patients with osteoporosis compared with healthy controls²⁹. Shen et al. showed that the expression of lncRNA *HOTAIR* in osteoporosis patients was significantly higher than that in normal people. They found *HOTAIR* suppressed osteogenic differentiation of rat BMSCs through inhibiting the Wnt/ β -catenin pathway³⁰. Yang et al. demonstrated that

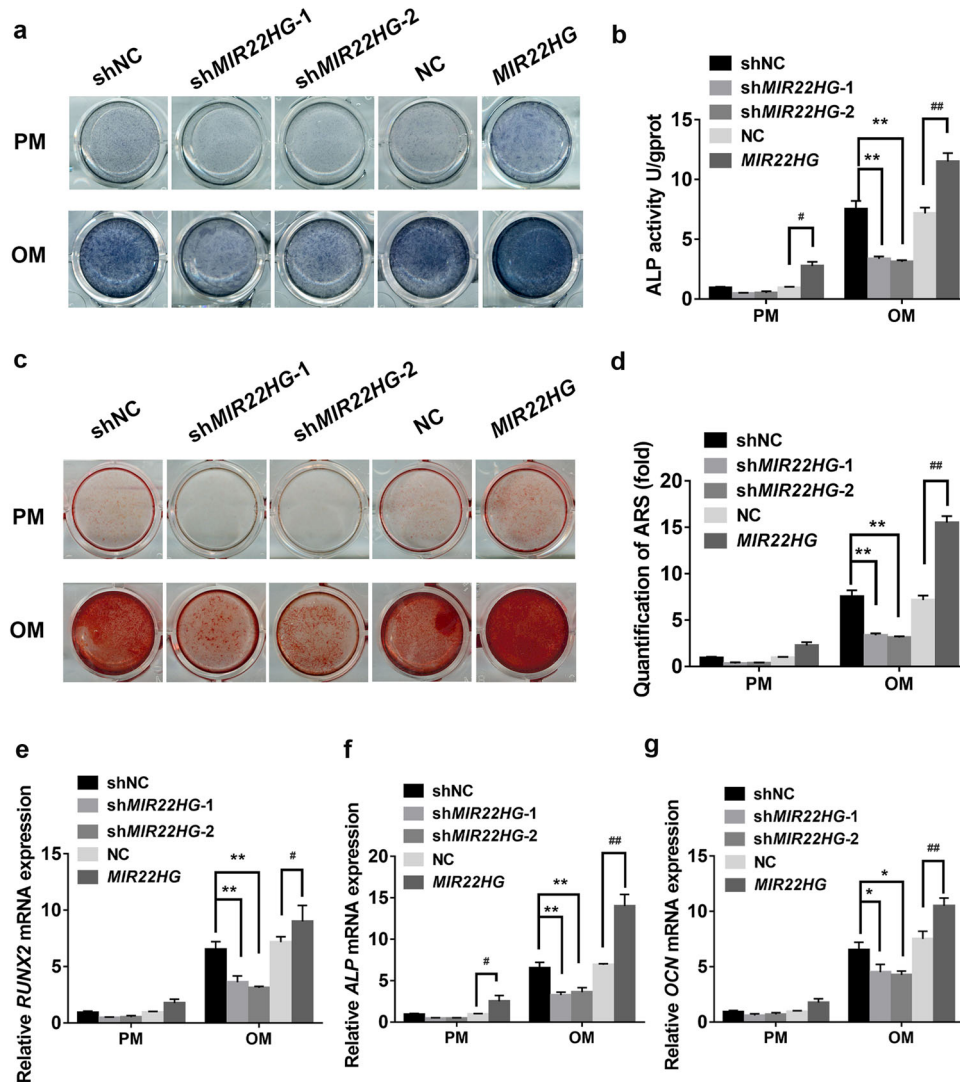


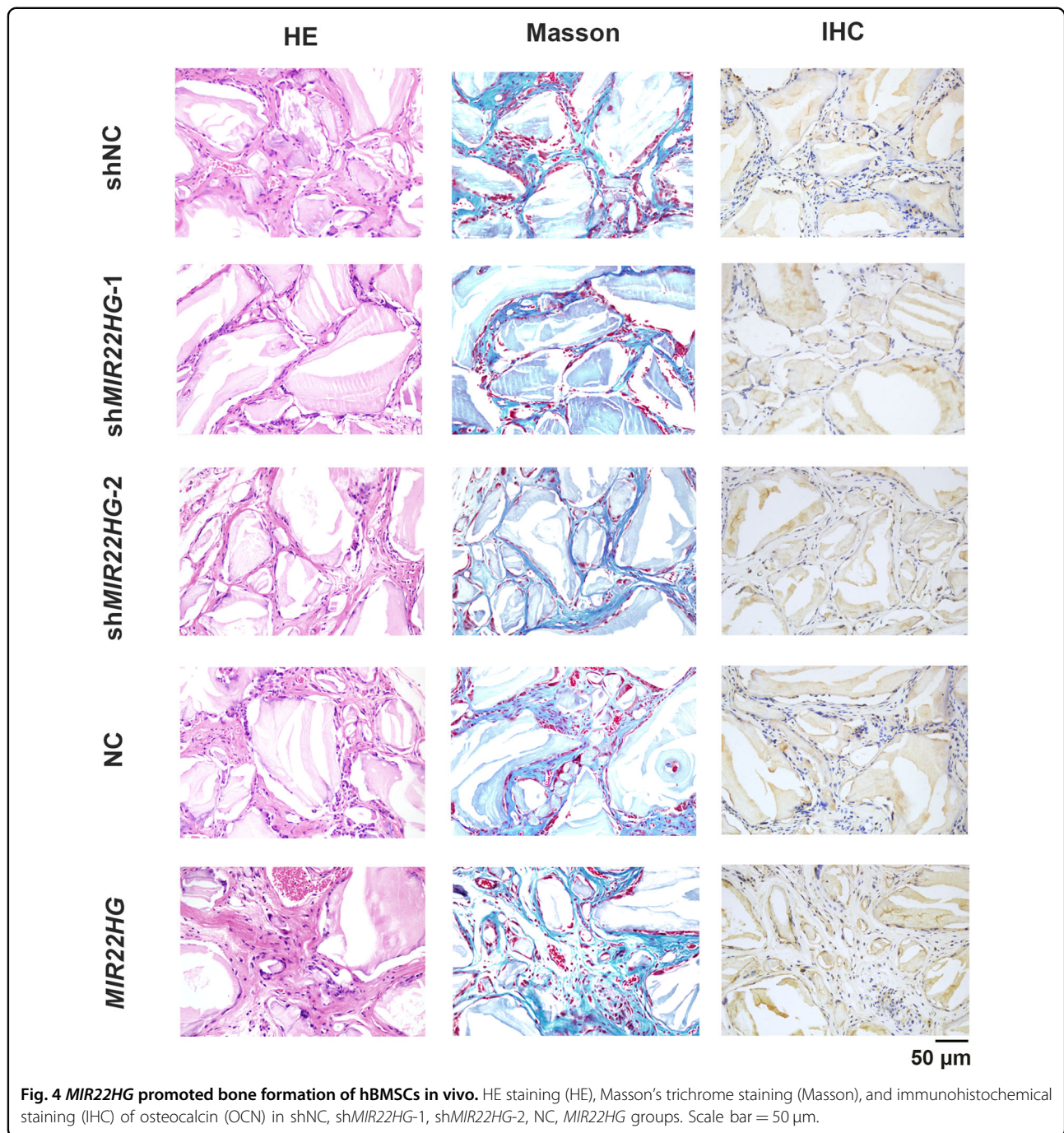
Fig. 3 The role of *MIR22HG* in osteogenic differentiation of hBMSCs. **a** Images of ALP staining in shNC, sh*MIR22HG*-1, sh*MIR22HG*-2, NC, *MIR22HG* groups. Cells were treated with proliferation medium (PM) or osteogenic medium (OM) for 7 days. **b** Histogram showing 7d ALP activity. **c, d** Alizarin Red S (ARS) staining and quantification in shNC, sh*MIR22HG*-1, sh*MIR22HG*-2, NC, *MIR22HG* groups on day 14. **e–g** Relative mRNA expression levels of *RUNX2*, *ALP*, and *OCN* measured by qRT-PCR on day 14 of osteogenic induction. *GAPDH* was used for normalization. Results are presented as the mean \pm SD, */# $p < 0.05$, **/# $p < 0.01$, * compared with shNC, # compared with NC.

lncRNA *ORLN1* alleviated osteoporosis by enhancing osteogenesis through the increase of BMP2 by sponging miR-140-5p³¹.

In our research, we examined the relative level of *MIR22HG* in mouse model of osteoporosis and found the expression of *MIR22HG* was lower compared with SHAM mice. We observed that *MIR22HG* was upregulated during the osteogenic differentiation of hBMSCs. Thus, we investigated the role of *MIR22HG* in regulating osteogenic differentiation. We found *MIR22HG* knockdown significantly inhibited osteogenesis, while *MIR22HG* over-expression enhanced osteogenesis of hBMSCs both

in vitro and in vivo. These results implied the positive effect of *MIR22HG* in osteogenic differentiation.

Various studies have provided evidence that the PI3K/AKT signaling plays an important role in regulating bone development. PI3K/AKT is negatively modulated by PTEN³². The loss of PTEN function in osteoblasts leads to persistent AKT activation, and subsequently increased osteogenic differentiation³³. Previous studies discovered that several lncRNAs interacted with AKT pathway in the process of osteogenic differentiation. For example, Wu et al. showed that lncRNA *HIF1A-AS2* promoted osteogenic differentiation of adipose-derived stem cells through



activating the PI3K/AKT signaling pathway³⁴. Zhang et al. reported that AKT signaling was involved in lncRNA *NKILA*-mediated osteogenic differentiation in mesenchymal stem cells³⁵.

In the current research, we found *MIR22HG* overexpression increased p-AKT expression, and the enhancing effect of *MIR22HG* overexpression on osteogenesis was abrogated by LY294002 or pcDNA3.1(+)-PTEN transfection. Moreover, *MIR22HG* knockdown inhibited

osteogenesis of hBMSCs and downregulated the phosphorylation level of AKT. The addition of 740 Y-P or si-PTEN reversed the inhibitory effect of *MIR22HG* knockdown on osteogenesis of hBMSCs. These results revealed that *MIR22HG* affected osteogenic differentiation of hBMSCs by modulating PTEN/AKT pathway.

Studies have shown that the intracellular distribution of lncRNAs is associated with their function and potential molecular roles³⁶. Thus, we detected the subcellular

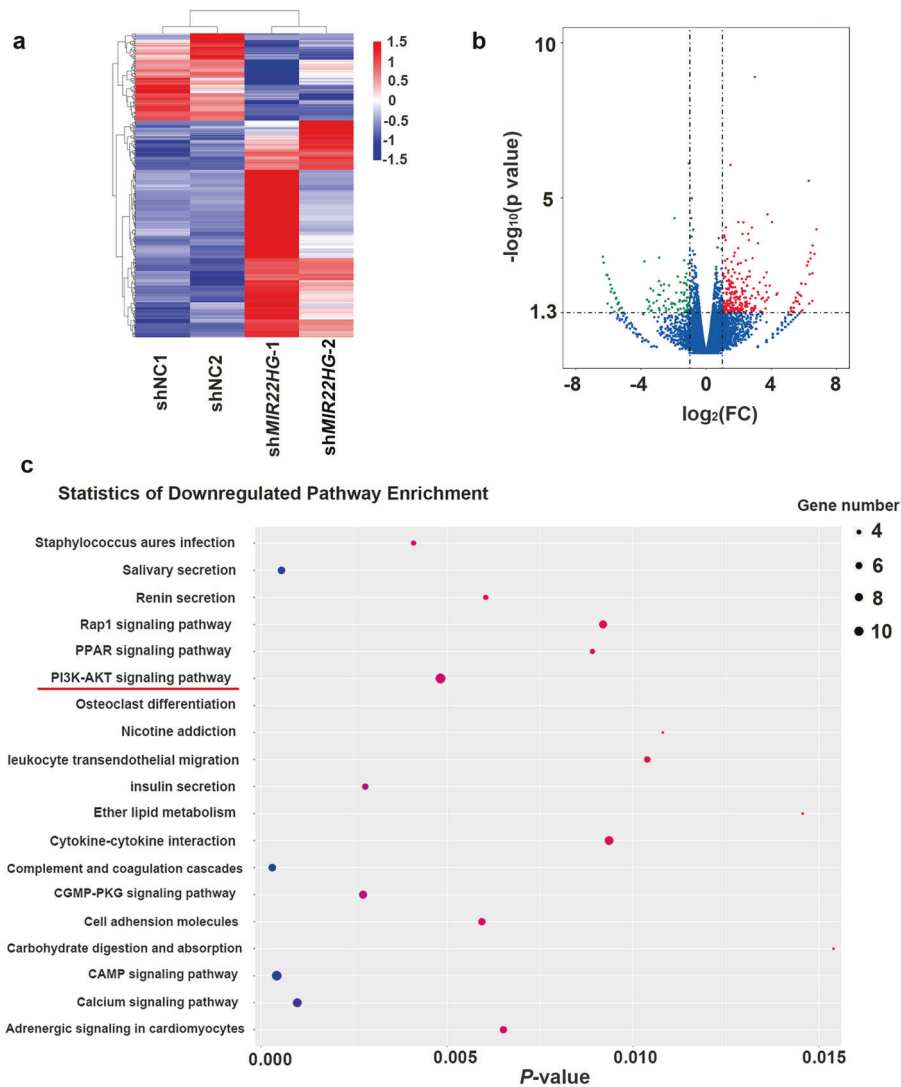


Fig. 5 Differential expression of genes between *MIR22HG* knockdown and shNC hBMSCs. **a** The differentially expressed genes in *MIR22HG* knockdown hBMSCs were shown in the heat map. p value <0.05 and fold change >2 were set as restrictive conditions to identify the differentially expressed genes. **b** The differentially expressed genes were counted; among these genes, a total of 278 genes were upregulated and 112 genes were downregulated. **c** KEGG pathway analysis showed the genes downregulated by *MIR22HG* knockdown might be related to different pathways, among which the top-ranking enriched pathways were shown.

localization of *MIR22HG* by FISH and subcellular fractionation assay. The results all revealed that *MIR22HG* was primarily located in the nucleus of hBMSCs. However, this result was contrary to a previous study, which found that *MIR22HG* was mostly located in the cytoplasm of lung cancer cell lines¹². This discrepancy may suggest that the role of *MIR22HG* varies between different cell types. To investigate the relationship between distribution of *MIR22HG* and PTEN/AKT pathway, we performed fluorescence colocalization microscopy analysis and observed that *MIR22HG* was mainly distributed in the nucleus while PTEN was presented both in the nucleus and cytoplasm. PTEN has been verified to play various

roles in different cellular compartments. Multiple studies have confirmed that cytoplasmic PTEN is an antagonist of the PI3K/AKT pathway because of its lipid phosphatase activity against PIP3. Recently, growing evidence demonstrates that nuclear PTEN is important for maintaining genomic stability through critical roles in modulating DNA repair and cell-cycle arrest³⁷. Although several components of the PI3K/AKT pathway also existed in the nucleus, such as PI3K, PIP3 and AKT, cytoplasmic but not nuclear pools of PIP3 have been discovered to be sensitive to the lipid phosphatase activity of PTEN³⁸. With the rapid development of high-throughput sequencing, a number of miRNAs were

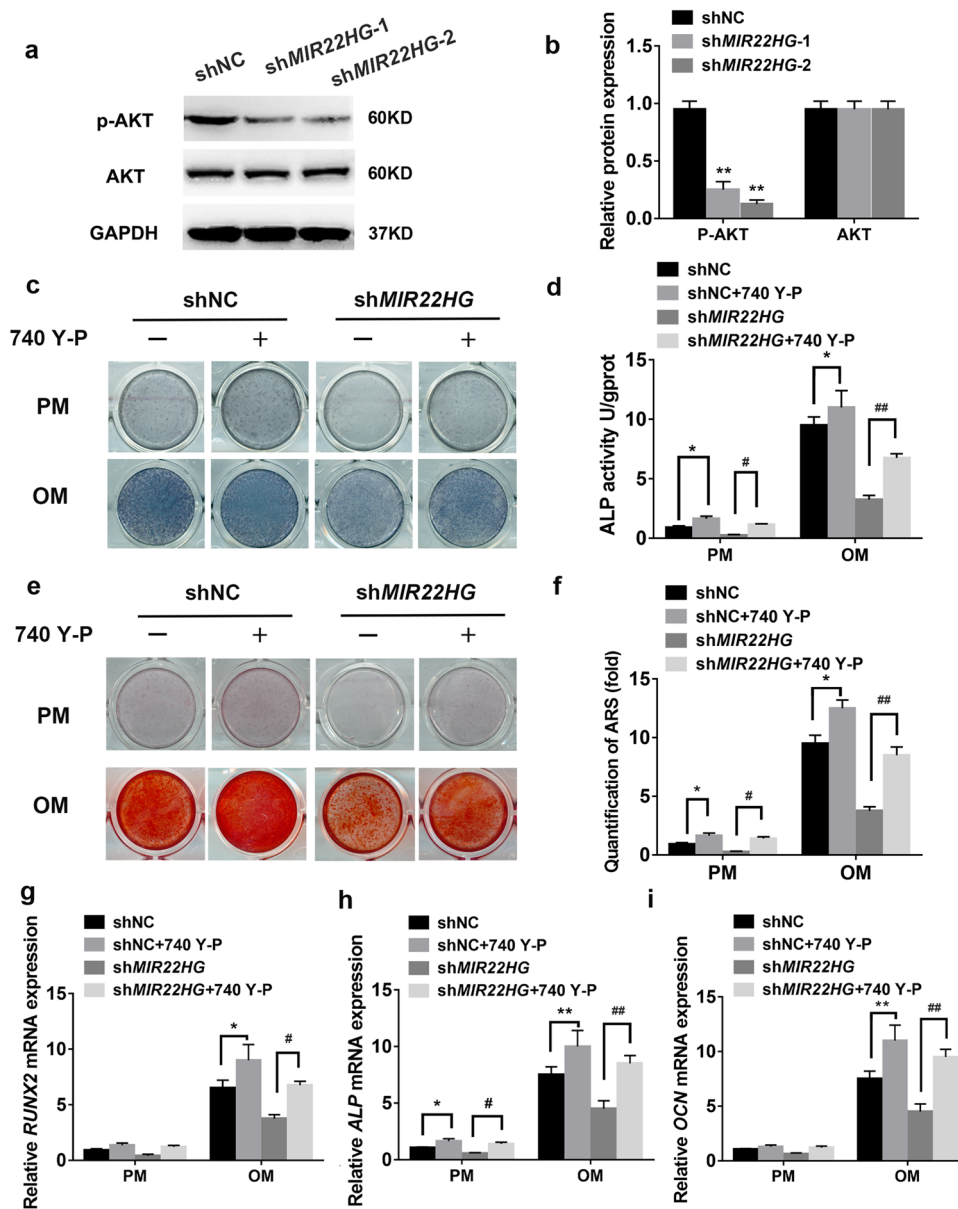


Fig. 6 *MIR22HG* knockdown inhibited AKT signaling. **a** The expression levels of total AKT and phosphorylated AKT (p-AKT) in shNC, sh*MIR22HG*-1, and sh*MIR22HG*-2 groups. GAPDH was used as an internal control. **b** The band intensities of **a** were analyzed by Image J software. **c** *MIR22HG* knockdown (sh*MIR22HG*) and the control (shNC) hBMSCs were treated with proliferation or osteogenic media for 7 days. 740 Y-P (10 μM) or DMSO (control '-') was added to the medium for 7 days and ALP staining was performed. **d** Histogram showing 7d ALP activity. **e** Images of Alizarin red S staining (ARS) in shNC, sh*MIR22HG* groups treated with 740 Y-P (10 μM) or DMSO (control '-') for 14 days. **f** Histograms showing quantification of ARS by spectrophotometry. **g-i** Relative mRNA expression levels of *RUNX2*, *ALP*, and *OCN* on day 14 after osteogenic induction. 740 Y-P (10 μM) was incubated for 14 days. DMSO was used as control. Results are presented as the mean ± SD, */#*p* < 0.05, **/#*p* < 0.01, * compared with shNC, # compared with sh*MIR22HG*.

identified to be involved in PTEN downregulation. miR-22 has been proved to downregulate PTEN in many different cell types via directly binding to the 3'UTR of PTEN^{39,40}. In this study, we found *MIR22HG* overexpression significantly promoted miR-22 expression in hBMSCs. Based on these results, we speculated that *MIR22HG* might regulate PTEN through miR-22. More

experimental studies are needed to further confirm this viewpoint.

Osteoporosis results from an imbalance between osteoblast-mediated bone formation and osteoclast-mediated bone resorption. In this study, we also examined the function of *MIR22HG* in osteoclastogenesis and found *MIR22HG* promoted osteoclast differentiation of

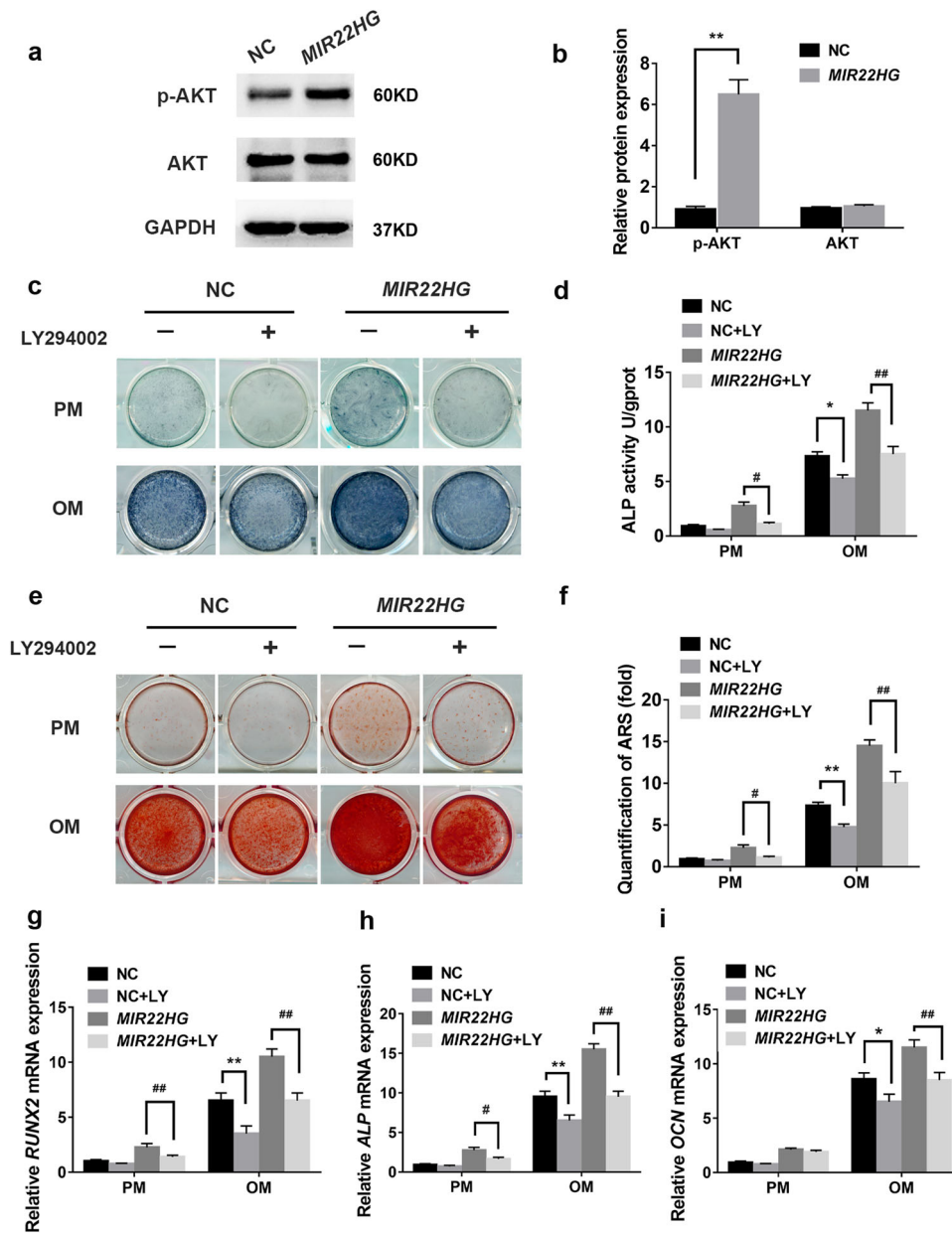


Fig. 7 *MIR22HG* overexpression activated AKT signaling. **a** The expression levels of total AKT and phosphorylated AKT (p-AKT) in NC, *MIR22HG* groups. GAPDH was used as an internal control. **b** The band intensities of **a** were analyzed by Image J software. **c** ALP staining in *MIR22HG* overexpression (*MIR22HG*) and the control (NC) hBMSCs with or without LY294002 (10 μ M) treatment on day 7 of osteogenic induction. DMSO was used as control (-). **d** Histogram showing 7d ALP activity. **e** Calcium deposition in NC, *MIR22HG* groups treated with LY294002 (10 μ M) or DMSO (control '-') was observed by Alizarin Red S staining on day 14 of osteogenic induction. **f** Histograms showing quantification of ARS by spectrophotometry. **g-i** Relative mRNA expression of *RUNX2*, *ALP*, and *OCN* on day 14 after osteogenic induction. LY294002 (10 μ M) was incubated for 14 days. DMSO was used as control. Results are presented as the mean \pm SD, * $^{\#}p < 0.05$, ** $^{\#\#}p < 0.01$, * compared with NC, # compared with *MIR22HG*. LY: LY294002.

RAW264.7 cells. Sugatani et al. reported that PTEN overexpression inhibited RANKL-induced osteoclast differentiation⁴¹. Moon et al. demonstrated that AKT stimulated osteoclast differentiation via GSK3 β /NFATC1 signaling cascade⁴². In this study, we found that *MIR22HG* reduced the level of PTEN and activated AKT pathway. We

reasoned that *MIR22HG* might regulate osteoclastogenesis with an involvement of PTEN/AKT pathway. Future studies will try to characterize the potential interactions between *MIR22HG* and these pathways.

In summary, we found for the first time that lncRNA *MIR22HG* was downregulated in the osteoporotic model,

and *MIR22HG* overexpression promoted osteogenic differentiation of hBMSCs both in vitro and in vivo. These results suggested that *MIR22HG* might be utilized as a novel diagnostic and therapeutic target for osteoporosis.

Acknowledgements

This study was supported by the Chinese Postdoctoral Science Foundation (2018M631442) and National Science Foundation of China (81700938&81800942&81772876).

Author details

¹The Second Clinical Division of Peking University School and Hospital of Stomatology, 100081 Beijing, China. ²Central Laboratory, Peking University School and Hospital of Stomatology, 100081 Beijing, China. ³Department of Oral and Maxillofacial Surgery, Peking University School and Hospital of Stomatology, 100081 Beijing, China. ⁴Department of Orthodontics, Peking University School and Hospital of Stomatology, 100081 Beijing, China

Data availability

The authors declare that all data supporting the findings of this study are available within the paper and its supplementary information files.

Conflict of interest

The authors declare that they have no conflict of interest.

Publisher's note

Springer Nature remains neutral with regard to jurisdictional claims in published maps and institutional affiliations.

Supplementary Information accompanies this paper at (<https://doi.org/10.1038/s41419-020-02813-2>).

Received: 18 February 2020 Revised: 16 July 2020 Accepted: 16 July 2020

Published online: 30 July 2020

References

- Sakai, T., Honzawa, S., Kaga, M., Iwasaki, Y. & Masuyama, T. Osteoporosis pathology in people with severe motor and intellectual disability. *Brain Dev.* **42**, 256–263 (2020).
- Tang, C. H. Osteoporosis: from molecular mechanisms to therapies. *Int. J. Mol. Sci.* **21**, E714 (2020).
- Trivedi, H. D., Danford, C. J., Goyes, D. & Bonder, A. Osteoporosis in primary biliary cholangitis: prevalence, impact and management challenges. *Clin. Exp. Gastroenterol.* **13**, 17–24 (2020).
- Liu, Q. et al. In vitro cell behaviors of bone mesenchymal stem cells derived from normal and postmenopausal osteoporotic rats. *Int. J. Mol. Med.* **41**, 669–678 (2018).
- Ma, N., Tie, C., Yu, B., Zhang, W. & Wan, J. Identifying lncRNA-miRNA-mRNA networks to investigate Alzheimer's disease pathogenesis and therapy strategy. *Aging* **12**, 2897–2920 (2020).
- Gao, G. C., Yang, D. W. & Liu, W. LncRNA TERC alleviates the progression of osteoporosis by absorbing miRNA-217 to upregulate RUNX2. *Eur. Rev. Med. Pharmacol. Sci.* **24**, 526–534 (2020).
- Zhang, X. et al. Comprehensive analysis of lncRNA and miRNA expression profiles and ceRNA network construction in osteoporosis. *Calcif. Tissue Int.* **106**, 343–354 (2020).
- Wang, J. et al. The role of lncRNAs in osteogenic differentiation of bone marrow mesenchymal stem cells. *Curr. Stem Cell Res. Ther.* **15**, 243–249 (2020).
- Cai, W. L. et al. LncRNA LINC00707 promotes osteogenic differentiation of hBMSCs through the Wnt/ β -catenin pathway activated by LINC00707/miR-145/LRP5 axis. *Eur. Rev. Med. Pharmacol. Sci.* **24**, 18–28 (2020).
- Wang, Z., Huang, Y. & Tan, L. Downregulation of lncRNA DANCR promotes osteogenic differentiation of periodontal ligament stem cells. *BMC Dev. Biol.* **20**, 2 (2020).
- Zheng, S. et al. LncRNA MALAT1 inhibits osteogenic differentiation of mesenchymal stem cells in osteoporosis rats through MAPK signaling pathway. *Eur. Rev. Med. Pharmacol. Sci.* **23**, 4609–4617 (2019).
- Su, W. et al. Silencing of long noncoding RNA MIR22HG triggers cell survival/death signaling via oncogenes YBX1, MET, and p21 in lung cancer. *Cancer Res.* **78**, 3207–3219 (2018).
- Wu, Y. et al. LncRNA MIR22HG inhibits growth, migration and invasion through regulating the miR-10a-5p/NCOR2 axis in hepatocellular carcinoma cells. *Cancer Sci.* **110**, 973–984 (2019).
- Gao, L. et al. MIR22HG as a tumor suppressive lncRNA in HCC: a comprehensive analysis integrating RT-qPCR, mRNA-Seq, and microarrays. *Oncotargets Ther.* **12**, 9827–9848 (2019).
- Cui, Z., An, X., Li, J., Liu, Q. & Liu, W. LncRNA MIR22HG negatively regulates miR-141-3p to enhance DAPK1 expression and inhibits endometrial carcinoma cells proliferation. *Biomed. Pharmacother.* **104**, 223–228 (2018).
- Li, H. & Wang, Y. Long noncoding RNA (lncRNA) MIR22HG suppresses gastric cancer progression through attenuating NOTCH2 signaling. *Med. Sci. Monit.* **25**, 656–665 (2019).
- Hu, X., Tan, Z., Yang, Y. & Yang, P. Long non-coding RNA MIR22HG inhibits cell proliferation and migration in cholangiocarcinoma by negatively regulating the Wnt/ β -catenin signaling pathway. *J. Gene Med.* **21**, e3085–e3085 (2019).
- Han, M. et al. Interfering with long non-coding RNA MIR22HG processing inhibits glioblastoma progression through suppression of Wnt/ β -catenin signalling. *Brain* **143**, 512–530 (2020).
- Jin, C. et al. RAI3 knockdown enhances osteogenic differentiation of bone marrow mesenchymal stem cells via STAT3 signaling pathway. *Biochem. Biophys. Res. Commun.* **524**, 516–522 (2020).
- Jin, C. et al. Inhibition of SLC7A11 by sulfasalazine enhances osteogenic differentiation of mesenchymal stem cells by modulating BMP2/4 expression and suppresses bone loss in ovariectomized mice. *J. Bone Miner. Res.* **32**, 508–521 (2017).
- Jin, C., Wang, W., Liu, Y. & Zhou, Y. RAI3 knockdown promotes adipogenic differentiation of human adipose-derived stem cells by decreasing β -catenin levels. *Biochem. Biophys. Res. Commun.* **493**, 618–624 (2017).
- Jin, C. et al. Inhibition of lncRNA MIR31HG promotes osteogenic differentiation of human adipose-derived stem cells. *Stem Cells* **34**, 2707–2720 (2016).
- Xi, Y., Qi, Z., Ma, J. & Chen, Y. PTEN loss activates a functional AKT/CXCR4 signaling axis to potentiate tumor growth and lung metastasis in human osteosarcoma cells. *Clin. Exp. Metastasis* **37**, 173–185 (2020).
- Luo, S. et al. Divergent lncRNAs regulate gene expression and lineage differentiation in pluripotent cells. *Cell Stem Cell* **18**, 637–652 (2016).
- Bononi, A. & Pinton, P. Study of PTEN subcellular localization. *Methods* **77–78**, 92–103 (2015).
- Zhang, Y. et al. MicroRNA-22 promotes renal tubulointerstitial fibrosis by targeting PTEN and suppressing autophagy in diabetic nephropathy. *J. Diabetes Res.* **2018**, 4728645 (2018).
- Kikuta, J. & Ishii, M. Bone imaging: osteoclast and osteoblast dynamics. *Methods Mol. Biol.* **1763**, 1–9 (2018).
- Ju, C. et al. Mesenchymal stem cell-associated lncRNA in osteogenic differentiation. *Biomed. Pharmacother.* **115**, 108912–108912 (2019).
- Fei, Q. et al. Identification of aberrantly expressed long non-coding RNAs in postmenopausal osteoporosis. *Int. J. Mol. Med.* **41**, 3537–3550 (2018).
- Shen, J. J. et al. LncRNA HOTAIR inhibited osteogenic differentiation of BMSCs by regulating Wnt/ β -catenin pathway. *Eur. Rev. Med. Pharmacol. Sci.* **23**, 7232–7246 (2019).
- Yang, L. et al. The long non-coding RNA-ORLNC1 regulates bone mass by directing mesenchymal stem cell fate. *Mol. Ther.* **27**, 394–410 (2019).
- Yang, C. et al. miRNA-21 promotes osteogenesis via the PTEN/PI3K/Akt/HIF-1 α pathway and enhances bone regeneration in critical size defects. *Stem Cell Res. Ther.* **10**, 65–65 (2019).
- Nielsen-Preiss, S. M., Silva, S. R. & Gillette, J. M. Role of PTEN and Akt in the regulation of growth and apoptosis in human osteoblastic cells. *J. Cell Biochem.* **90**, 964–975 (2003).
- Wu, R. et al. Long non-coding RNA HIF1A-AS2 facilitates adipose-derived stem cells (ASCs) osteogenic differentiation through miR-665/IL6 axis via PI3K/Akt signaling pathway. *Stem Cell Res. Ther.* **9**, 348–348 (2018).
- Zhang, Y. et al. LncRNA NKILA integrates RXFP1/AKT and NF- κ B signalling to regulate osteogenesis of mesenchymal stem cells. *J. Cell Mol. Med.* **24**, 521–529 (2020).
- Batista, P. J. & Chang, H. Y. Long noncoding RNAs: cellular address codes in development and disease. *Cell* **152**, 1298–1307 (2013).

37. Dai, W. Unmasking PTEN's nuclear functions. *Cell Cycle* **15**, 3341–3342 (2016).
38. Lindsay, Y. et al. Localization of agonist-sensitive PtdIns(3,4,5)P₃ reveals a nuclear pool that is insensitive to PTEN expression. *J. Cell Sci.* **119**, 5160–5168 (2006).
39. Wang, X., Wang, Y., Kong, M. & Yang, J. MiR-22-3p suppresses sepsis-induced acute kidney injury by targeting PTEN. *Biosci. Rep.* **40**, BSR20200527 (2020).
40. Wang, L. et al. The microRNA miR-22 represses Th17 cell pathogenicity by targeting PTEN-regulated pathways. *Immunohorizons* **4**, 308–318 (2020).
41. Sugatani, T., Alvarez, U. & Hruska, K. A. PTEN regulates RANKL- and osteopontin-stimulated signal transduction during osteoclast differentiation and cell motility. *J. Biol. Chem.* **278**, 5001–5008 (2003).
42. Moon, J. B. et al. Akt induces osteoclast differentiation through regulating the GSK3 β /NFATc1 signaling cascade. *J. Immunol.* **188**, 163–169 (2012).